J Solid State Electrochem (2012) 16:1941–1952
DOI 10.1007/s10008-011-1593-3

ORIGINAL PAPER

Electrochemical studies of $LiMnPO_4$ as aqueous rechargeable lithium–ion battery electrode

H. Manjunatha · T. V. Venkatesha · G. S. Suresh

Received: 9 August 2011 / Revised: 3 November 2011 / Accepted: 10 November 2011 / Published online: 29 November 2011

Abstract A study of the electrochemical behavior of $LiMnPO_4$ prepared by RAPET method in different aqueous electrolytes using cyclic voltammetry (CV), galvanostatic charge–discharge experiments, and electrochemical impedance spectroscopy is reported. CV peak current is proportional to the square root of scan rate under 0.2 mV s^{-1}. The system satisfied the required conditions for a reversible system with a resistive behavior. $LiMnPO_4$ was found to undergo proton insertion at lower concentrations of electrolyte. At higher concentrations or saturated solutions of electrolytes, lithium insertion/de-insertion becomes the main reaction though the effect of proton insertion/de-insertion reaction cannot be ignored. Electrochemical insertion/de-insertion of lithium in $LiMnPO_4$ was studied using EIS technique. The kinetic parameter, charge transfer resistance (R_{ct}), obtained by simulating the experimental impedance data with an equivalent circuit showed a minimum at the potential close to the CV peak potential. The cell $LiTi_2(PO_4)_3$/5 M$LiNO_3$/$LiMnPO_4$ delivers a discharge capacity of 84 mAh g^{-1} in the first cycle at an applied current of 0.2 mA cm^{-2} and it retains its initial capacity over 50 cycles with good rate capability.

Keywords Lithium manganese phosphate · Aqueous rechargeable lithium batteries, · Lithium insertion/de-insertion reactions · Galvanostatic charge–discharge · EIS technique

H. Manjunatha · G. S. Suresh (✉)
Chemistry Research Centre, S. S. M. R. V. Degree College, Jayanagar,
Bangalore 560041, India
e-mail: sureshssmrv@yahoo.co.in

T. V. Venkatesha
Department of Chemistry, Kuvempu University, Jnanasahyadri,
Shankaraghatta 577451 Shimoga, India

Introduction

Lithium transition metal phosphates with ordered olivine structure, $LiMPO_4$ (M=Co, Mn, Fe, Cu) have attracted much attention as potential Li-ion battery cathode materials since the demonstration of reversible electrochemical lithium insertion extraction for $LiFePO_4$ in 1997 [1, 2]. Crystalline $LiMPO_4$ has an orthorhombic unit cell (D_{2h}^{16} – space group *Pmnb*) which accommodates four units of $LiMPO_4$. All the oxygen ions of phospho-olivines form strong covalent bonds with P^{5+} to form the PO_4^{3-} tetrahedral polyanion and stabilize the entire three-dimensional frameworks. This is responsible for the stable operation of these cathode materials at higher temperature [3, 4] and extreme safety under abusive conditions [1–5]. The P_{tet}–O–M_{oct} linkage in the structure induces the super exchange interaction that tunes the M^{3+}/M^{2+} redox energy to useful level (3.4 V for Fe^{3+}/Fe^{2+}, 4.1 V for Mn^{3+}/Mn^{2+}, and 4.8 V for Co^{3+}/Co^{2+}; all potentials are vs lithium metal). The high theoretical capacity of phospho-olivines up to 170 mAh g^{-1} provides high energy density compared to that of $LiCoO_2$, $LiNiO_2$, and $LiMn_2O_4$ [6]. All these factors make transition metal phosphates suitable for large applications such as electric vehicles where safety is of top priority. Significant efforts have been made on the substitution of Fe with Mn, Co, and Ni and to understand their suitability as cathode materials in lithium batteries [7–10].

$LiMnPO_4$ appears to be the best candidate among the $LiMPO_4$ family despite quite poor electrochemical performances reported so far in the non-aqueous battery systems [10–13]. It can theoretically deliver a higher energy density than its Fe counterpart due to the high redox potential of Mn^{3+}/Mn^{2+} vs Li/Li^+ (4.1 V). Moreover, $LiFePO_4$ suffers from its low electrical conductivity, because it is basically an electronic insulator [14], and small lithium diffusivity.

The literature on olivine-type $LiMnPO_4$ is limited to non-aqueous media, and studies in aqueous media are very rare. Manickam et al. [15] reported the preliminary investigations on the electrochemical behavior of $LiMnPO_4$ in saturated LiOH solution and showed $LiMnPO_4$ forms of $MnPO_4$ when electro-oxidized. This process is reversible. Recently, it has been reported that the addition of TiS_2 [16] additive to $LiMnPO_4$ leads to modification of the electrochemical performance of the cathode like improved de-lithiation/lithiation mechanism by suppressing the proton de-insertion/insertion reaction.

Cyclic voltammetry is a very useful tool in modern analytical chemistry. In this technique, a cyclic linear potential sweep is applied to the electrode and the resulting current is recorded. Information about the kinetics and mass transport can be obtained by analyzing the CV profiles. A redox couple in which both species (oxidant, O, and reductant, R) rapidly exchange electrons with the electrode are called an electrochemical reversible couple. A simple reversible redox system involves a single electron transfer in a solution medium where the rate of forward reaction and rate of backward reaction are in equilibrium. The following are few characteristics of such a reversible system.

1. The peak potential separation, $\Delta E_p = 0.058/n$ V at all scan rates at 25 °C.
2. The ratio of the cathodic to anodic peak currents is unity, i.e., $i_{pa}/i_{pc} = 1$.
3. The peak current is proportional to the square root of scan rate, i.e, i_p (diffusion-controlled process) $\propto \nu^{1/2}$.

The peak current is related to diffusion coefficient as shown in Eq. 1:

$$i_p = 0.446F(F/RT)^{1/2}C^*\nu^{1/2}AD^{1/2} \quad (1)$$

CV profiles rarely satisfy the above three characteristics for a reversible system in practical experiments. This may be due to slow electron transfer kinetics which arises from the solution resistance and resistance offered by solid state reaction. Especially the systems which involve lithium intercalation/de-intercalation are more complicated than solution-based systems owing to the fact that the electrode material itself undergoes reaction with the transport of lithium ions into and out of the electrode's active material.

In our present study, we report the electrochemical characterization and electrochemical performance of $LiMnPO_4$ synthesized by RAPET method in aqueous electrolytes as a part of our ongoing project on aqueous rechargeable lithium batteries. RAPET method is a simple, low-temperature, and economical approach for the synthesis of nanosized materials, carbon-coated metal oxide particles, magnetic particle encapsulated in carbon shells and magnetic nanoparticles, etc. [17–20]. Our work presented here on $LiMnPO_4$ will focus on studying the reversibility of lithium insertion/de-insertion reaction, the effect of concentration of electrolyte, and the nature of electrolyte. This study of the electrochemical intercalation/de-intercalation of Li ions involved using electrochemical impedance spectroscopy (EIS) and constructing an aqueous rechargeable lithium battery using $LiMnPO_4$ as cathode, LiV_3O_8 as anode, and 5 M $LiNO_3$ as electrolyte. Stability of $LiMnPO_4$ in aqueous electrolyte is another concerning factor. In addition, the effect of coupled reactions like proton de-insertion/insertion along with lithium ions cannot be ruled out. Therefore, a detailed knowledge of the electrochemical properties of $LiMnPO_4$ is necessary in order to use it as a cathode material in aqueous rechargeable lithium batteries.

Experimental

Synthesis of materials

$LiMnPO_4$ used in this study was synthesized by RAPET method. In a typical procedure, stoichiometric amounts of $NH_4H_2PO_4$, Li_2CO_3, and MnO_2 are mixed. The mixture was ground, pressed into a pellet, and taken in a Swagelok. It was then fired at 700 °C for 10 h in a tubular furnace. The rate of heating and cooling was maintained at 10 °C / min. $LiTi_2(PO_4)_3$ was also synthesized by the same method and was used as anode material. The synthesized samples were characterized by X-ray powder diffraction (XRD) using Philips X'pert Pro Diffractometer (Cu K radiation, secondary graphite monochromator). All of the reagents used were from Sigma–Aldrich and used as received.

The working electrode was prepared on a stainless steel mesh current collector. The SS mesh was sand-blasted to remove the surface oxide layer and to generate a rough surface. The SS mesh of 2.23-cm^2 geometric surface areas with a tag for electrical connection was etched in dil. HNO_3, cleaned with detergent, washed with pure water, rinsed with acetone, dried, and weighed. $LiMnPO_4$, acetylene black, and polytetrafluoroethylene were ground in a mortar with a weight ratio of 80:10:10. Slurry was prepared by adding a few drops of *N*-methyl-2-pyrrolidinone. The slurry was then coated on to the previously weighed SS mesh and dried at 110 °C for 12 h under vacuum. Electrochemical measurements were carried out in a glass cell of 25-ml capacity using LiOH, $LiNO_3$, or Li_2SO_4 aqueous solutions as electrolytes, Pt foil as counter electrode, and a saturated calomel electrode (SCE) as the reference electrode. All potential values are reported against SCE. Cyclic voltammetry, galvanostatic charge–discharge, and EIS experiments were performed using BioLogic potentiostat–galvanostat instrument. The amplitude of the AC perturbation was 10 mV in the frequency range 100 kHz to 5 mHz.

Results and discussion

The crystal phase of the $LiMnPO_4$ sample synthesized by RAPET method for this work is found to be an ordered olivine structure indexed by orthorhombic *Pnmb* as evidenced from the powder XRD experiments as shown in Fig. 1. No impurities were detected with the XRD. The XRD pattern obtained here is in good agreement with that reported in literature for $LiMnPO_4$ [1, 10, 15]. Figure 1 also shows the X-ray diffraction pattern of Nasicon $LiTi_2(PO_4)_3$ prepared by RAPET method. The material is in pure phase according to its XRD pattern. $LiTi_2(PO_4)_3$ has a rhombohedral (space group, *R3c*) structure with an open three-dimensional framework of TiO_6 octahedra sharing all corners with PO_4 tetrahedra and vice versa. Li^+ ions occupy the interstitial spaces either 18e or 6b sites. All diffraction lines are indexed based on rhombohedral structure.

Cyclic voltammetry of $LiMnPO_4$ in aqueous solutions

Figure 2a shows the CV profiles of stainless steel (SS) mesh current collector and $LiMnPO_4$ in saturated LiOH electrolyte. The figure clearly shows that the current peaks which correspond to oxygen evolution and hydrogen evolution are not observed on the SS mesh electrode within the potential window in which the cyclic voltammogram of $LiMnPO_4$ is recorded. This shows that the saturated LiOH electrolyte provides a stable electrochemical window for the lithium intercalation/de-intercalation in $LiMnPO_4$. The CV profile of $LiMnPO_4$ consists of a reduction peak C_1 at −0.625 V and its corresponding anodic peak A_1 at −0.188 V. In addition to the anodic peak A_1, a small peak, A_2, has been observed at −0.402 V during the scan in anodic direction. This is ascribed to proton de-insertion, which is not reversible [16]. The large potential gap of 0.437 V between the oxidation and reduction peaks suggested that the electron transfer process is very slow in aqueous saturated LiOH solution. Thus, the synthesized $LiMnPO_4$ material undergoes electro-oxidation/reduction reactions presumably involving a change in the oxidation state of Mn atom in $LiMnPO_4$. Figure 2b shows the changes in the CV profile when $LiMnPO_4$ is subjected to

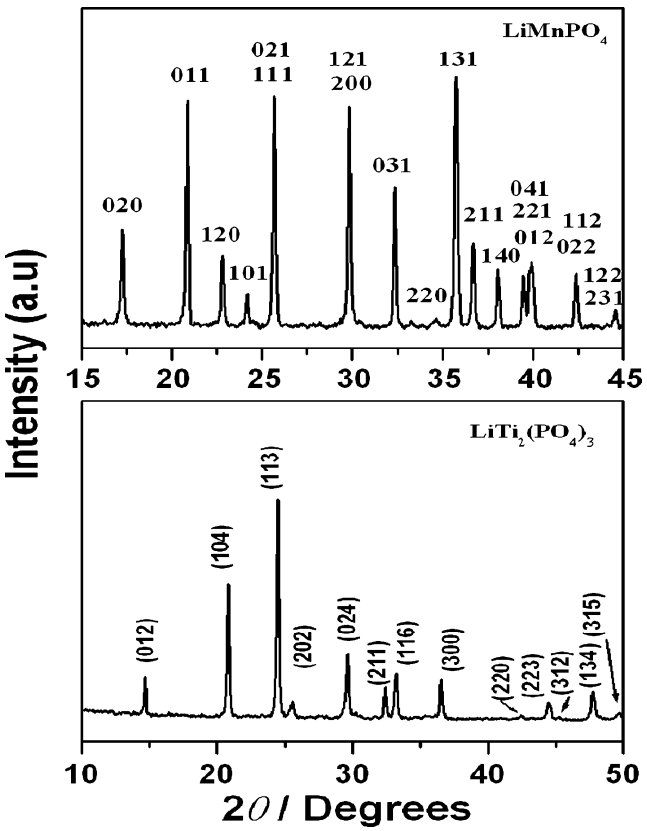

Fig. 1 X-ray diffraction patterns of synthesized $LiMnPO_4$ and $LiTi_2(PO_4)_3$ electrode materials

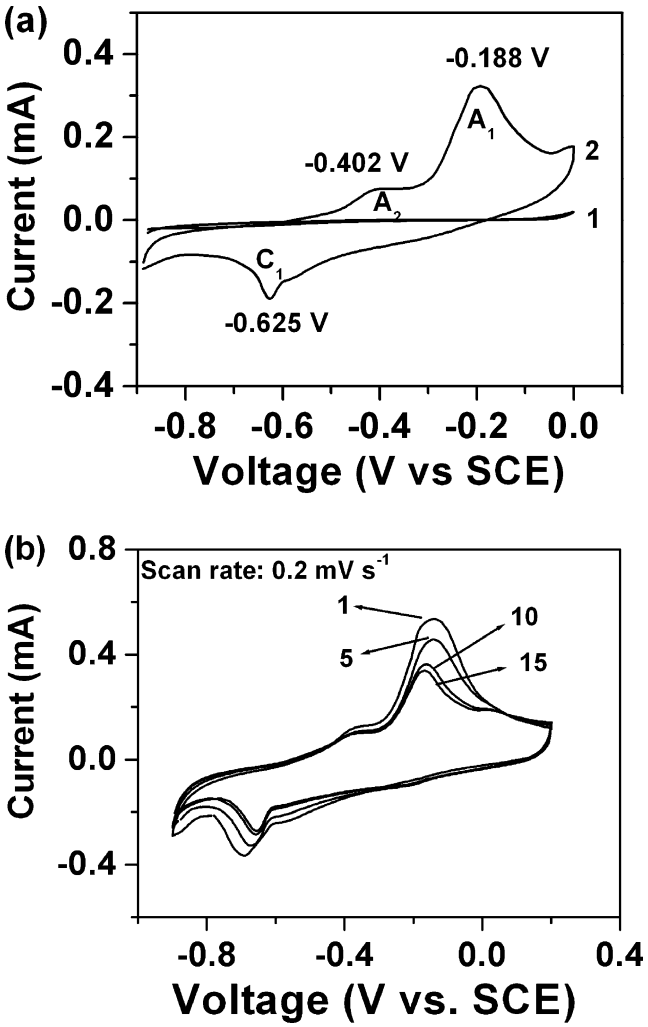

Fig. 2 **a** CV profile of SS mesh current collector (*1*) and $LiMnPO_4$ (*2*) in saturated LiOH electrolyte (scan rate, 0.1 mV s^{-1}). **b** Cyclic voltammogram of $LiMnPO_4$ in saturated LiOH electrolyte for 1st, 5th, 10th, and 15th cycles (scan rate, 0.2 mV s^{-1})

continuous cycling (15 cycles) in the potential region −0.90 V to +0.20 V at a scan rate of 0.2 mV s^{-1}. The cathodic and anodic currents decreased slightly up to the 10th cycle and then tend to stabilize, suggesting that the material could be reversibly reduced/oxidized over a number of cycles. For comparison, we have also recorded cyclic voltammograms of both anode and cathode materials in organic electrolyte, $LiPF_6$/EC-DMC. Figure 3a shows the cyclic voltammogram of $LiMnPO_4$ in 1 M$LiPF_6$/EC-DMC organic electrolyte. It exhibits an anodic peak at 4.09 V vs Li^+/Li and a cathodic peak at 3.20 V vs Li^+/Li corresponding to lithium de-intercalation and intercalation, respectively .The peak potential difference (ΔE_p) is about 890 mV at a scan rate of 0.1 mV s^{-1}. This difference in the redox peak potentials of $LiMnPO_4$ in organic electrolyte is more compared to 437 mV in saturated LiOH (Fig. 2a) measured at the same scan rate. The narrow faradaic peaks observed in saturated LiOH compared to that in non-aqueous 1 M$LiPF_6$/EC-DMC electrolyte clearly indicate the fast electrochemical kinetics in aqueous electrolytes. On the other hand, Fig. 3b shows the CV profile of $LiTi_2(PO_4)_3$ in 1 M$LiPF_6$/EC-DMC electrolyte. It exhibits an anodic peak at 2.50 V and a cathodic peak at 2.17 V vs lithium with a peak potential separation of 330 mV.

Effect of scan rate

To study the reversibility of $LiMnPO_4$ system, the scan rate was varied between 25 μV s^{-1} and 0.6 mV s^{-1}. The following observations can be made from the CV profiles as shown in Fig. 4a at different scan rates: (a) the peak separation increases with increasing scan rate, (b) a linear dependence during the initial increase in current–potential behavior, and (c) all the CV profiles overlap regardless of the scan rate at the beginning of charging and discharging.

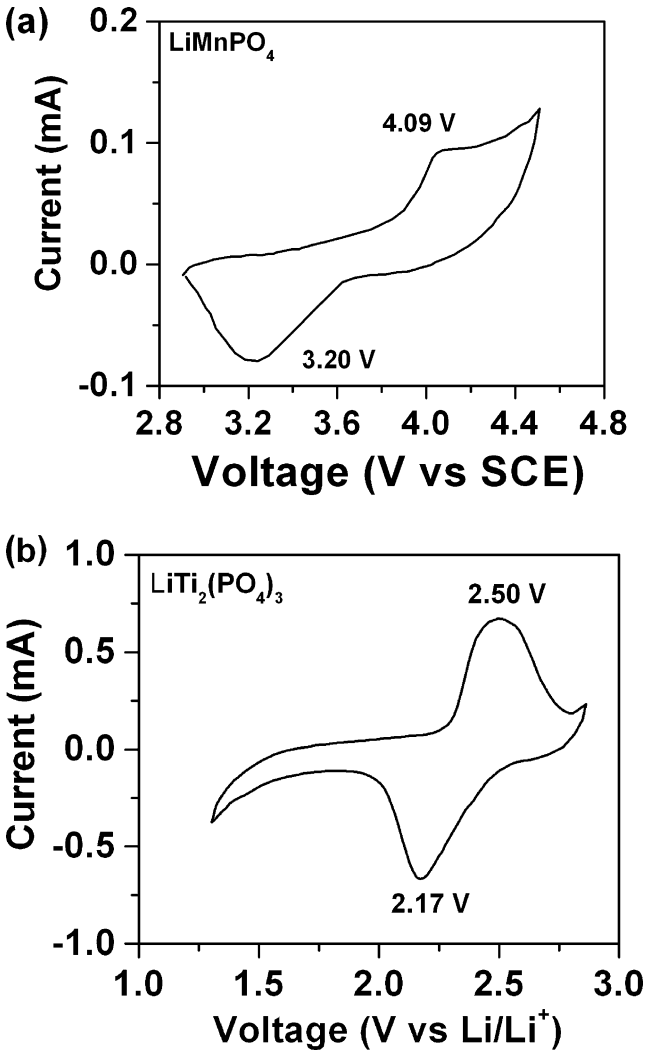

Fig. 3 **a** CV profile of $LiMnPO_4$ and **b** $LiTi_2(PO_4)_3$ in 1 M $LiPF_6$/EC-DMC (scan rate, 0.2 mV s^{-1})

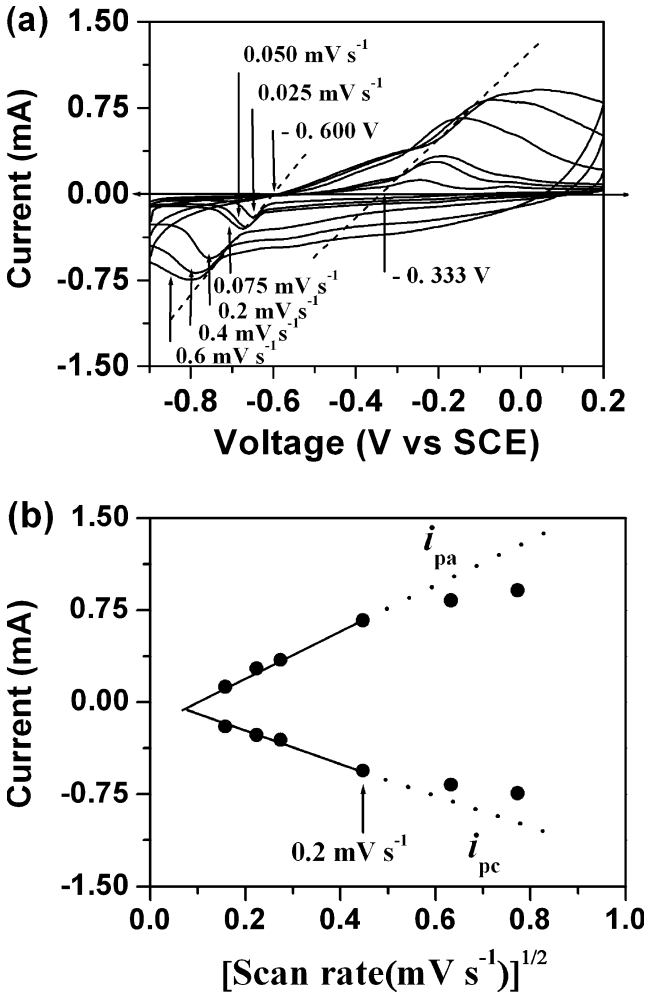

Fig. 4 **a** CV profiles of $LiMnPO_4$ at different scan rates (*dashed lines* are the extrapolations of the initial current potential lines to the *x*-axis). **b** Graph of peak currents vs square root of the scan rate

The first two observations indicate that the initial current is a linear function of the potential of the electrode. Figure 4b shows the plot of anodic and cathodic peak currents with square root of scan rate. The plot shows two regions: a linear dependence between i_p and $\nu^{1/2}$ for scan rates less than 0.2 mV s^{-1} (solid line) and a deviation from straight-line relation for scan rates of more than 0.2 mV s^{-1} (dashed line). As mentioned in the introductory part, reversible reactions have $i_p \propto \nu^{1/2}$ relationship (characteristic 3). This suggests that the thin $LiMnPO_4$ electrode has a critical scan rate of 0.2 mV s^{-1} for reversibility at 25 °C.

In theory, we can apply an extremely small scan rate to get the true separation between the anodic and cathodic peaks. Practically, we applied 25 μV s^{-1} as the lowest scan rate. The peak potential difference is about 0.409 V which is too large to compare with the theoretical value of 0.059 V for a one-electron transfer system to be reversible (characteristic 1). The reason for this large potential gap is ascribed to the very slow electron transfer process at $LiMnPO_4$ in aqueous LiOH solution [16]. Characteristic 2 specifies that the anodic and cathodic peak currents have the same magnitude. However, Fig. 4b shows that this condition is not satisfied at all scan rates in the case of $LiMnPO_4$, i.e., $i_{pc}/i_{pa} \neq 1$. At low scan rates (up to 0.2 mV s^{-1}), the ratio of i_{pc}/i_{pa} is almost equal to unity. However, for higher scan rates (more than 0.2 mV s^{-1}), $i_{pc}/i_{pa} \neq 1$.This is due to the fact that $LiMnPO_4$ undergoes a two-phase process during charge and discharge. Li^+ ions are most likely to be transported through regions with $MnPO_4$ or $LiMnPO_4$ [21, 22]. This difference in the electrochemical environment for Li movement may account for the difference in the magnitude of the peak currents at higher scan rates. Thus, we conclude that characteristic 2 need not be upheld for $LiMnPO_4$ system especially since the integrated area under the cathodic and anodic scans is almost same (i.e., the same capacities of about 84 mAh g^{-1} for charging and discharging). Combining all the information from the above discussions, we conclude that the CV profiles of $LiMnPO_4$ show a reversible reaction with a resistive behavior similar to the work reported for $LiFePO_4$ in non-aqueous electrolytes [23]. Chemical diffusion coefficients of Li^+ are calculated by cyclic voltammetry using Eq. 2. The cyclic voltammograms at scan rates 25, 50, and 75 μV s^{-1} in Fig. 4b are used to calculate the Li^+ diffusion coefficient. According to Eq. 2, the diffusion coefficient of lithium ions of $LiMnPO_4$ is found to be 1.648×10^{-13} cm^2 s^{-1}, close to the reported data for $LiMnPO_4$ in organic electrolytes [24]. This shows that the diffusion of lithium ions does not change much since it occurs in the solid bulk of the electrode material which remains the same $LiMnPO_4$ in the presence of aqueous or non-aqueous electrolytes.

Identification of cation

It is interesting to identify the cation de-intercalated/intercalated from/to $LiMnPO_4$ upon the redox reaction of Mn^{2+}/Mn^{3+} couple. The electrochemical lithium ion de-intercalation/intercalation reaction has already been proved for $LiMnPO_4$ in aqueous electrolytes [15]. The corresponding equations for the redox peaks of $LiMnPO_4$ in Fig. 2a can be written as follows:

$$\text{Oxidation} : LiMnPO_4 \rightarrow Li^+ + MnPO_4 \quad (2)$$

$$\text{Reduction} : Li^+ + MnPO_4 \rightarrow LiMnPO_4 \quad (3)$$

According to Nernst law, the oxidation and reduction reactions should follow the dependence of the formal potential (E_f) of the redox reaction on the activity of the lithium ion (a_{Li+}) in accordance with the following equation:

$$E_f = E^\circ + 0.059 \log a_{Li+} \quad (4)$$

i.e., the E_f of the redox reaction should be directly proportional to the logarithm of the lithium activity in the LiOH aqueous solutions. The cyclic voltammetry curves of $LiMnPO_4$ electrode in various concentrations of LiOH, viz, 0.05, 0.1, 0.5, 1, and 2 M and finally in saturated LiOH, are as shown in Fig. 5a. As seen in the figure, the CV profile obtained in 0.05 M LiOH shows an oxidation peak at about −0.350 V and a cathodic peak at about −0.460 V with a formal potential of −0.426 V. The anodic and cathodic peak currents are also low. In 0.1 MLiOH electrolyte, $LiMnPO_4$ shows similar behavior in the CV profile with a formal potential of around −0.355 V. However, as the concentration of the electrolyte increases to 0.5 M, there is a significant change in the CV profile. Both the cathodic and anodic currents increased with a shift in the peak potentials towards the positive side. The cathodic peak is found to be having two submerged peaks. As the concentration of the electrolyte increased further to 1 and 2 M, the corresponding CV peaks show decreased peak currents, peak potential separation, and formal potential. The formal potential (values of E_f) increases with increase in concentration of LiOH electrolyte up to 0.5 M and then it decreases. The reason for this decreased formal potential (expected to increase) is discussed in the next paragraph. In 1 M, 2 M, and saturated LiOH, mainly one pair of redox peaks appeared with decreased peak currents. The redox peak potentials shift in the negative direction.

To confirm the nature of cation ion inserted/extracted to/from $LiMnPO_4$, we plotted the relationship between the formal potential, E_f, and the logarithm of activity of lithium ions in different concentrations of LiOH as shown in

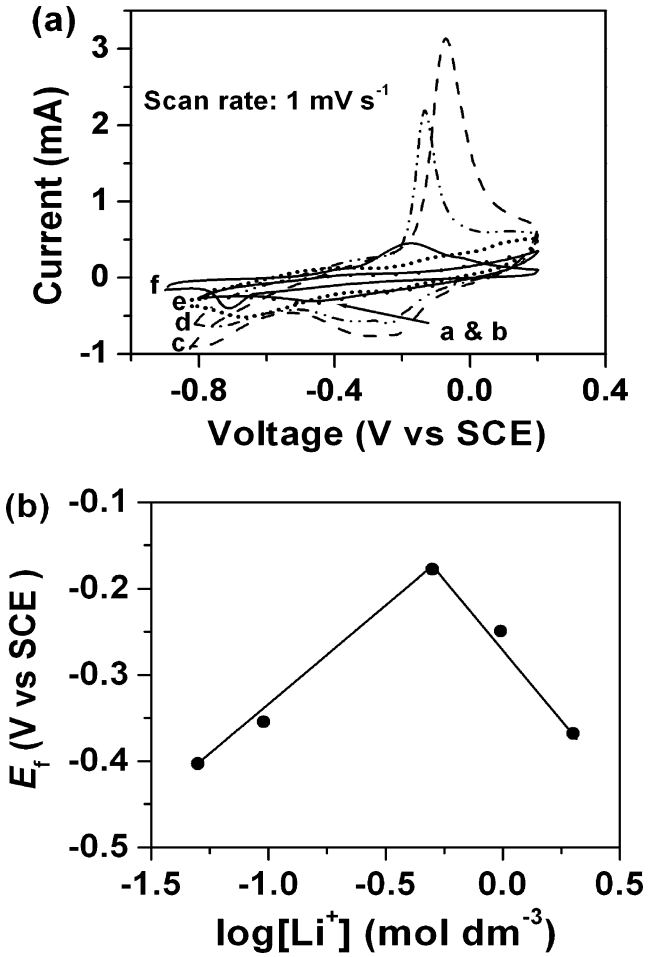

Fig. 5 **a** Cyclic voltammograms of $LiMnPO_4$ in different concentrations of LiOH electrolyte solution. *a*, 0.05 M; *b*, 0.1 M; *c*, 0.5 M; *d*, 1 M; and *e*, 2 M. Scan rate, 1 mV s^{-1}. **b** Derived plot of E_f vs log [Li^+]

Fig. 5b. Almost a straight line with a positive slope proves that the redox peaks on the CV profile of $LiMnPO_4$ in LiOH aqueous electrolyte are due to lithium ion de-insertion/insertion reactions. However, it is interesting to note that the shapes of the CV profiles obtained in various concentrations of LiOH are not similar and they do not represent a single redox reaction taking place at $LiMnPO_4$ electrode. It is evident from the CV profiles that proton insertion/de-insertion reaction may be coupled with lithium insertion/de-insertion reaction. As the concentration of LiOH increases, the influence of proton insertion/de-insertion reaction on that of lithium ion decreases and is minimum or negligible in saturated LiOH. Thus, the anodic and cathodic peak currents decrease. This accounts for the shapes of the CV profiles in different concentrations of LiOH. The decreased E_f values in Fig. 5b for 1 and 2 M LiOH are explained as follows. At these higher concentrations of LiOH, Li^+ insertion/de-insertion becomes the main redox reaction though proton insertion/de-insertion reaction cannot be ignored. The negative shift of cathodic peak is reported for $LiMnPO_4$ [16], where it is proposed that the negative shift in the cathodic peak is due to decreased interference of proton insertion /de-insertion reaction and is assigned mainly to lithium insertion reaction.

Study of electrochemical lithium intercalation/de-intercalation of lithium into/from $LiMnPO_4$ in saturated LiOH electrolyte

Electrochemical impedance spectroscopy is used to study the mechanism of lithium intercalation/de-intercalation into/from $LiMnPO_4$. Figure 6a shows the impedance spectra as Nyquist plots measured at various potentials during charge. Qualitatively, all of the spectra have the following features: a strongly potential dependent semicircular arc in the high frequency region (HFS) which corresponds to charge transfer process, a Warburg element in the low frequency region describing the solid state diffusion of lithium ions, and a steep line at lower frequencies which describe the capacitive behavior of the electrode. This blocking-type electrode behavior is generally seen for thin film electrodes and is due to the limited diffusion of lithium ions in the solid state. Formation of surface electrolyte interface (SEI) layer in non-aqueous lithium battery systems is a common observation and the semicircular arc in the high frequency region is usually assigned to the diffusion of lithium ions through this SEI layer. In aqueous electrolytes, the formation of SEI is not extensively proved. In fact, it is reported that SEI layer is not formed in the presence of aqueous electrolytes, or even if it is formed the resistance offered by such an ultra-thin layer is negligible [25–28].

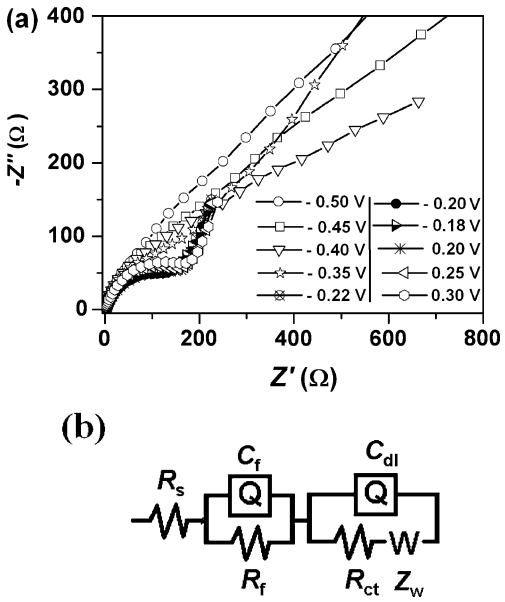

Fig. 6 **a** Impedance spectra of $LiMnPO_4$ as Nyquist plots measured at 25 °C during charge at various potentials as indicated in the figure. **b** The equivalent circuit used to simulate the experimental impedance data

Table 1 Kinetic parameters as a function of potential during charge process

E (V)	R_s (Ω)	R_{ct} (Ω)	C_{dl} (mF)	I_0 (mA)	Z_w (Ω)
−0.45	0.416	293.6	1.34	0.087	0.0057
−0.40	0.413	282.6	1.40	0.090	0.0075
−0.35	0.415	116.7	5.70	0.220	0.0122
−0.22	0.427	107.2	2.90	0.239	0.0291
−0.20	0.422	109.3	2.60	0.234	0.0314
−0.18	0.403	135.4	3.10	0.189	0.033
0.20	0.447	171.1	3.60	0.150	0.0111
0.25	0.444	171.9	3.60	0.149	0.0004
0.30	0.436	184.2	4.00	0.139	0.0002

Therefore, in general, the HFS observed in the impedance spectra of insertion electrode materials in the presence of aqueous electrolytes is assigned to the charge transfer process. However, Sinha et al. [29] have reported the formation of SEI layer on $LiCoO_2$ electrode in the presence of 5 M$LiNO_3$ aqueous electrolyte and have assigned the HFS to the migration of lithium ions through the surface passivating layer. In the present study, we could not simulate the experimental impedance spectra with a simple modified Randle's equivalent circuit which does not take into account the migration of lithium ions through the SEI layer. The equivalent circuit as shown in Fig. 6b was used to simulate the experimental impedance spectra during both charge and discharge. The pure capacitor in the equivalent circuit is replaced by constant phase element (Q). Constant phase elements are used when the impedance spectra exhibit a low-frequency dispersion due to porosity or roughness of the electrode surface [30]. This equivalent circuit consists of two RC circuits in series, one of which is for the charge transfer process as pointed out earlier. The part of the circuit which describes the charge transfer process has the following elements: resistance for charge transfer (R_{ct}), a CPE corresponding to double layer capacitance (Q_{dl},), a Warburg element (Z_W) corresponding to lithium ion diffusion in the solid state, and a resistance (R_s) for the solution resistance. The parallel circuit, R_fC_f, in the equivalent circuit must be assigned either to the migration of lithium ions through the SEI layer or to the bulk capacity and resistance. A careful observation of the impedance spectra during both charge and discharge does not support the idea of SEI layer formation (except in Fig. 8b during discharge, where a potential independent semicircular arc is found in the high frequency region). We believe that this must be due to the bulk capacity and resistance as evidenced from the known fact that saturated LiOH electrolyte has low conductivity. However, a detailed further study of this electrode–electrolyte interface is required to establish facts. Initially, the diameter of the semicircular arc is so high that it is hardly seen as shown in Fig. 6a (from −0.50 to −0.40 V) owing to fact that the absence of charge transfer process or current flow is negligible in this potential region. As the potential approaches the CV peak potential, the capacitive lines disappear and a clear semicircular arc begins to appear in the potential range between −0.35 to −0.20 V. The dimension of the semicircular arc is found to be sensitive to the electrode potential in this potential region. Both the magnitude of the arc and the total cell impedance dramatically drop, revealing the lithium ion diffusion process. Contrary to this, the impedance spectra measured between −0.18 to 0.30 V show an increase in the magnitude of the semicircular arc, leading to increase in the total cell impedance and attainment of limited ion mass transport regime. The values of kinetic parameters calculated from the impedance data during charge and discharge processes are summarized in Tables 1 and 2, respectively. The parameters of the equivalent circuit from fitting the experimental impedance data of $LiMnPO_4$ electrode with charging potential are shown in Fig. 7. R_s stays constant at 0.420 Ω as expected because solution composition and thus conductance remains constant. R_{ct} decreases with the charging potential and reaches a minimum value at E_{SCE}= −0.22 V, which corresponds to CV peak potential and then increases. Correspondingly, the exchange current I_0 ($I_0=RT/nFR_{ct}$) increases with the charge voltage and reaches a maximum value at −0.22 V when the charge transfer resistance is low and then decreases. From the CV curve in Fig. 2a, it can be seen that this potential −0.22 V is close to the anodic peak potential (E_a=−0.188 V), implying favorable kinetic conditions for lithium de-intercalation reaction. C_{dl} increases gradually with voltage. C_{dl} represents double-layer capacitance of the electrode–solution interface. It is a function of electrode potential and does not

Table 2 Kinetic parameters as a function of potential during discharge process

E (V)	R_s (Ω)	R_{ct} (Ω)	C_{dl} (mF)	I_0 (mA)	Z_w (Ω)
−0.35	0.440	282.8	3.10	0.090	0.030
−0.45	0.444	291.2	1.47	0.088	0.028
−0.55	0.440	305.2	1.13	0.084	0.031
−0.60	0.441	305.9	1.12	0.080	0.024
−0.62	0.430	317.7	1.16	0.086	0.006
−0.64	0.428	298.2	1.20	0.089	0.002
−0.66	0.432	288.2	1.24	0.126	0.0002
−0.68	0.434	202.8	1.59	0.344	0.00002
−0.72	0.433	74.45	2.00	0.397	0.0050
−0.76	0.436	64.56	2.30	0.210	0.00431
−0.80	0.439	121.8	2.50	0.090	0.0046

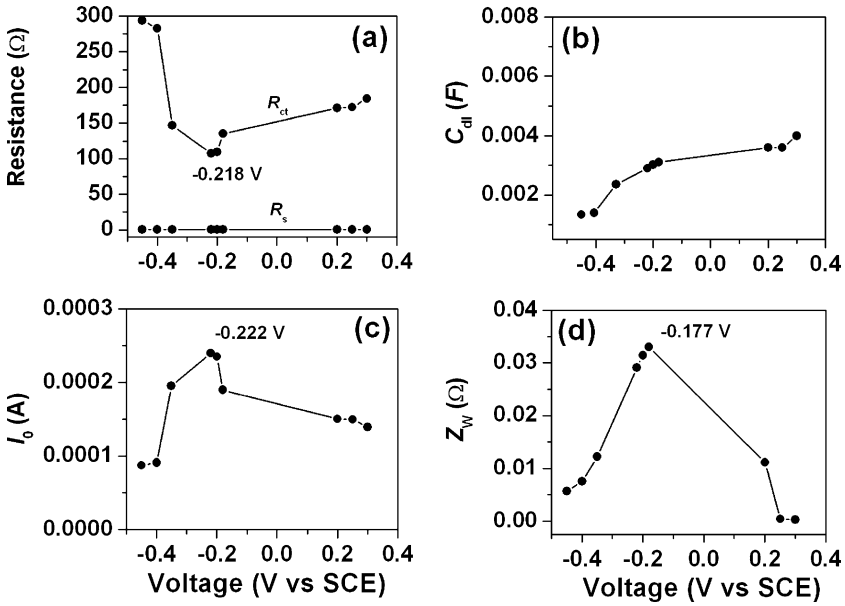

Fig. 7 **a**–**d** Relationship between kinetic parameters with charge voltage vs SCE

behave like a simple capacitor. C_{dl} changes during lithium insertion/de-insertion in $LiMnPO_4$ at higher and lower potentials. This could be due to the large volume change of the host material. Figure 8a, b show the Nyquist plots of $LiMnPO_4$ electrode obtained during discharge at various potentials. The same trend in the variation of impedance spectra is observed as discussed for that during charge. Figure 9 shows the variation kinetic parameters obtained by fitting the experimental impedance data obtained during discharge. R_s stays constant at 0.440 Ω. R_{ct} and Z_w shows the same trend during discharge. They increase at the beginning of lithium intercalation and then they reach minimal values at −0.760 V (R_{ct}) and −0.676 V (Z_w). The C_{dl} decreases gradually as lithium ion intercalates into $LiMnPO_4$ and then reaches to a minimum value of 1 mF at E_{SCE}=−0.60 V. Subsequently, the value of C_{dl} increases gradually. A similar type of trends in the variations of kinetic parameters have been reported for LiV_3O_8 [31] and $LiCoO_2$ [32] lithium insertion materials in aqueous lithium electrolytes.

Effect of different electrolytes

Figure 10 shows the CV profiles of $LiMnPO_4$ obtained in different electrolytes. The CV profiles change with the type of electrolyte solution. The CV profile is broadest for the electrode in saturated LiOH with high viscosity and low conductivity. The potential gap between the redox peaks is small in 5 M $LiNO_3$ and the peak current is also enhanced. The redox peak positions are in the negative side in the case of saturated $LiNO_3$, whereas in 2 M Li_2SO_4 and 5 M $LiNO_3$ they tended to shift in the positive direction. In 5 M $LiNO_3$ electrolyte, both the oxidation and reduction peaks appear on the positive potential side with an oxidation peak at 0.95 V and a reduction peak at 0.55 V vs SCE.

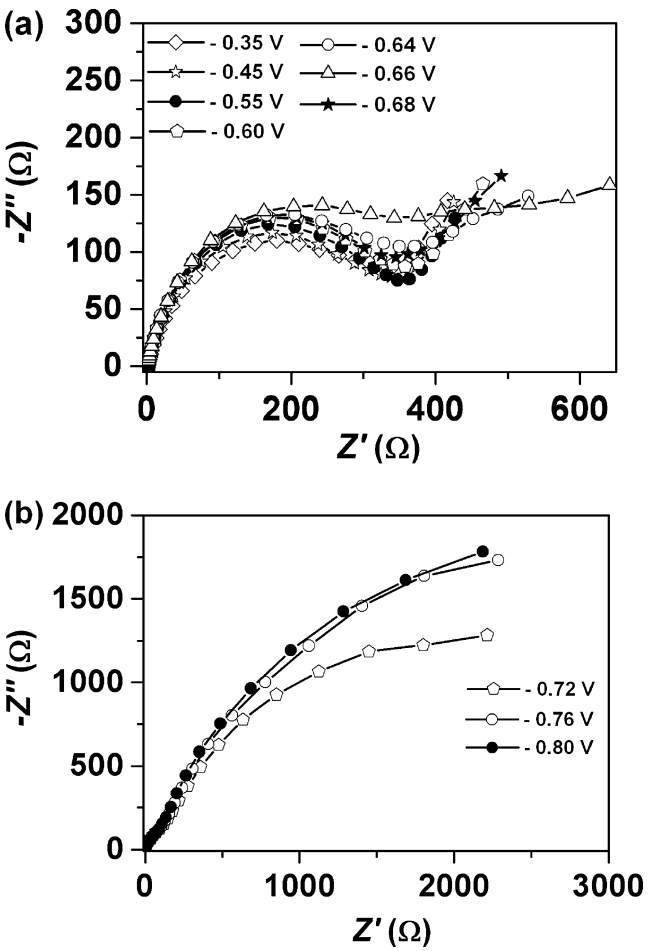

Fig. 8 **a**, **b** Impedance spectra of $LiMnPO_4$ as Nyquist plots measured at 25 °C during discharge at various potentials as indicated in the figure

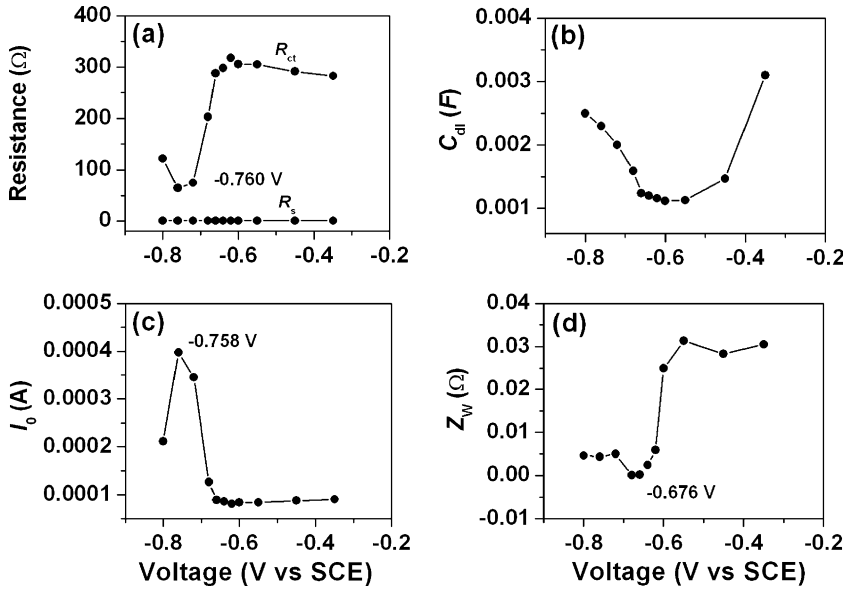

Fig. 9 **a–d** Relationship between kinetic parameters with discharge voltage vs SCE

Charge–discharge studies

In literature, the electrochemical cell performance of Zn/$LiMnPO_4$ which uses saturated LiOH containing 0.1 mol dm^{-3} $ZnSO_4$ electrolyte is reported [15, 16]. The metallic zinc has been used as anode to construct an aqueous rechargeable lithium battery with $LiMnPO_4$ as cathode. From the previous section on the cyclic voltammetry study of $LiMnPO_4$ in saturated LiOH (see Fig. 2a), it is well understood that $LiMnPO_4$ exhibits a pair of redox peaks located at −0.188 V (oxid. A_1) and −0.625 V (red. C_1) versus SCE, which is evidently due to the lithium intercalation and de-intercalation reaction accompanying gain and loss of an electron. The average redox potential is −0.406 V. Since the redox potential of $LiMnPO_4$ appears in the negative potential region vs SCE in saturated LiOH electrolyte, the electrochemical cell constructed using $LiTi_2(PO_4)$ (which also has redox peaks in the negative potential region) as anode did not undergo charging and discharging processes in our present work. Probably for this reason, the authors of [15, 16] have used Zn as anode material with $LiMnPO_4$ cathode in saturated LiOH electrolyte. As discussed earlier, in 5 M$LiNO_3$ electrolyte, $LiMnPO_4$ exhibits a pair of redox peaks located at 0.95 V (oxi) and 0.55 V (red) vs. SCE with an average redox potential of 0.75 V (positive potential region). This is evidently due to the intercalation and de-intercalation reaction accompanying gain and loss of an electron. These voltages are well within the voltage for oxygen evolution. This illustrates that $LiMnPO_4$ can be used as positive electrode with $LiTi_2(PO_4)_3$ as negative electrode (which has an average negative redox peak potential of −0.418 V vs SCE) in 5 M$LiNO_3$.

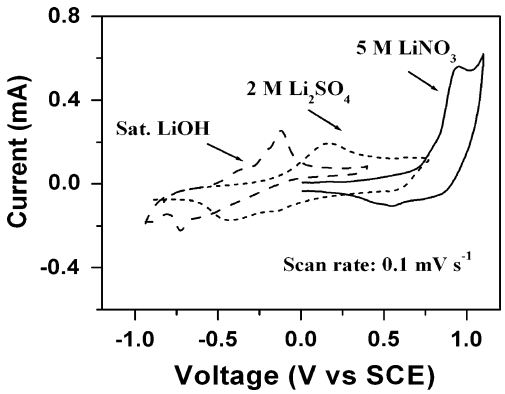

Fig. 10 Comparison of cyclic voltammograms of $LiMnPO_4$ in different electrolytes. Scan rate, 0.1 mV s^{-1}

Figure 11 shows the cyclic voltammograms of $LiTi_2(PO_4)_3$ and $LiMnPO_4$ in 5 M$LiNO_3$ aqueous electrolyte. The electrochemical stability window of the SS mesh current collector (CV profile of SS mesh) is also shown in

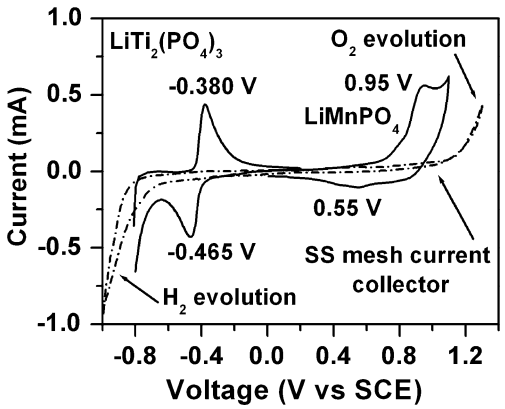

Fig. 11 Cyclic voltammograms of $LiMnPO_4$ and $LiTi_2(PO_4)_3$ in 5 M $LiNO_3$ aqueous electrolyte. Scan rate, 1 mV s^{-1}. Also, see the stable potential window of aqueous solution on SS mesh electrode

the figure. The redox potentials of both electrode materials are well within the stable potential window of the aqueous solution. The charge–discharge curves of $LiTi_2(PO_4)_3$/5 M $LiNO_3$/$LiMnPO_4$ between the voltage range 0 and 1.5 V are as shown in Fig. 12a. The discharge capacity of 84 mAh g^{-1} is obtained at the applied current of

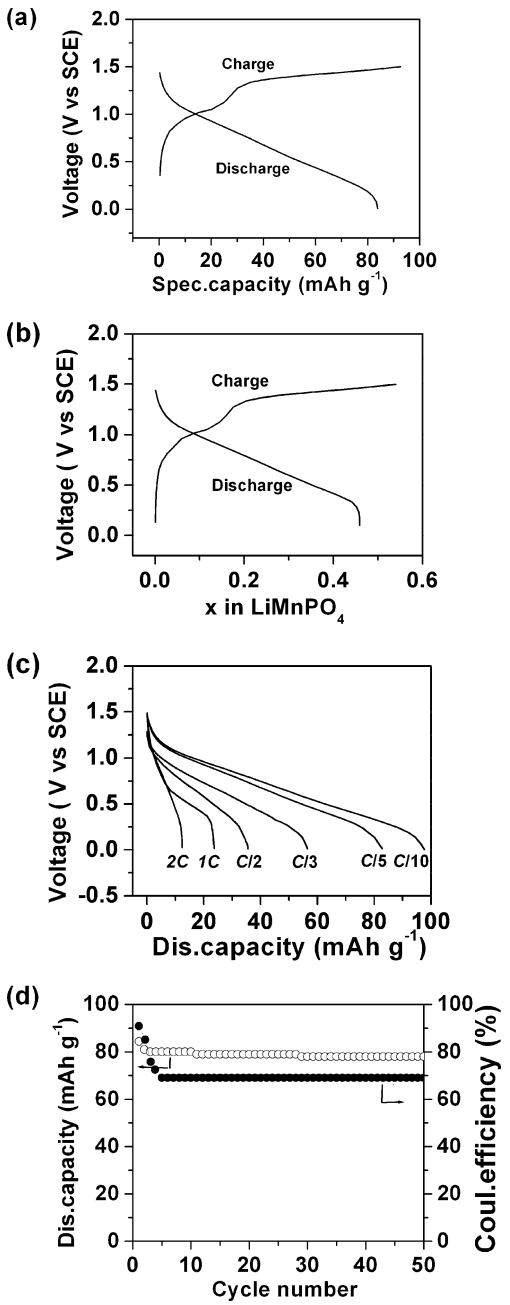

Fig. 12 **a** Typical charge and discharge curves $LiTi_2(PO_4)_3$ /$LiMnPO_4$ cell for the second cycle in 5 M$LiNO_3$ aqueous electrolyte. Applied current was 0.2 mA cm^{-2} between 0 and 1.5 V. **b** *x* in $LiMnPO_4$ vs potential, *E*. **c** Initial discharge profiles for the $LiTi_2(PO_4)_3$ /$LiMnPO_4$ cell in 5 M$LiNO_3$ at different C_{rates}, as indicated in the graph, at room temperature. **d** Capacity trend vs. number of cycles at $C/3_{rate}$ and coulombic efficiency vs number of cycles

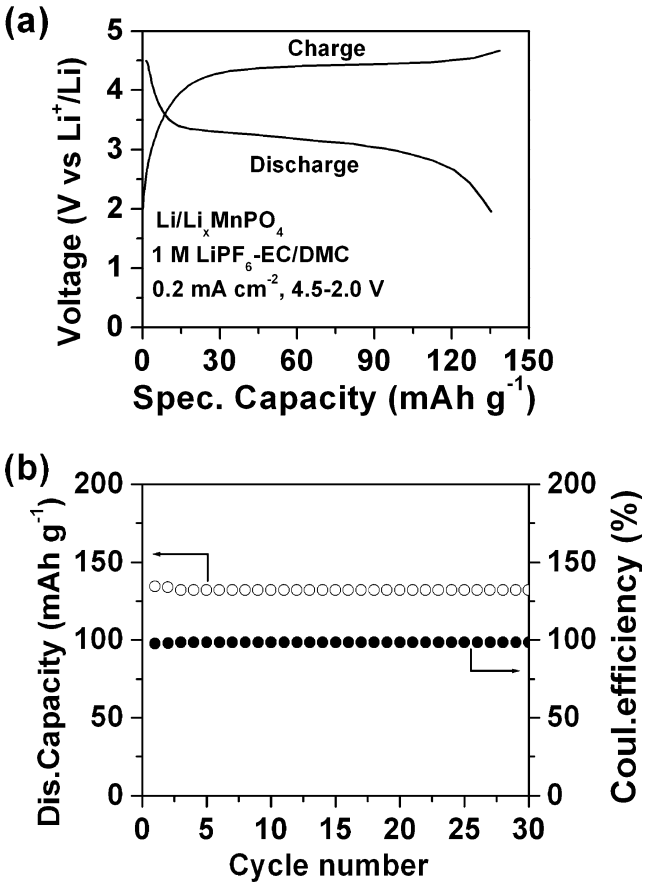

Fig. 13 **a** Typical charge and discharge curves Li/$LiMnPO_4$ cell for the second cycle in 1 M$LiPF_6$/EC-DMC electrolyte. Applied current was 0.1 mA cm^{-2} between 2.0 and 4.5 V. **b** Capacity trend vs. number of cycles at $C/3_{rate}$ and coulombic efficiency vs number of cycles

0.2 mA cm^{-2}. During charging process, a slight inflection around 1.2 V is observed. This could be due to the twinning effect caused by the de-lithiation in the olivine structure [15]. However, during the discharge process, no such inflection was seen. There is a single plateau up to 0.25 V and then it decreases drastically to the discharge cutoff voltage of 0 V. The shapes of the charge and discharge curves appear to be different. However, the cell can be

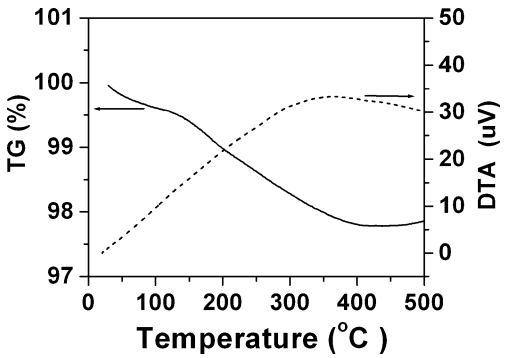

Fig. 14 TGA and DTA curves of $LiMnPO_4$ recorded at a heating rate of 10 °C min^{-1}

reversibly charged and discharged. The theoretical capacity for $LiMnPO_4$ is reported as 170 mAh g^{-1} in non-aqueous electrolytes [23]. The amount of lithium de-intercalated from $LiMnPO_4$ is found to be 0.54 at an applied current of 0.2 mA cm^{-2} ($C/5_{rate}$). The amount of lithium intercalated during the subsequent discharge is slightly less (0.45) compared to that during charging. This observation is again confirmed from the plot of x in $LiMnPO_4$ vs E as shown in Fig. 12b. The cell $LiTi_2(PO_4)_3$/5 M$LiNO_3$/$LiMnPO_4$ is subjected to charge–discharge cycling at various C_{rates}. Figure 12c shows the discharge curves. The discharge capacity decreases at high C_{rates} and about 20% of the theoretical capacity is retained at $C/2_{rate}$. Cycling behavior of the cell has been studied at $C/3_{rate}$. Figure 12d shows the results over 50 cycles. Both the measured capacities and coulombic efficiency of each cycle are shown. After the first five cycles, the discharge capacity and the coulombic efficiency are stabilized. The discharge capacity dropped by 20% during the first few cycles, after which it was stabilized. Figure 13 shows the charge–discharge performance of Li/$LiMnPO_4$ cell in 1 M$LiPF_6$/ EC-DMC electrolyte. It can be seen that the Li/$LiMnPO_4$ cell delivers a discharge capacity of 135 mAh g^{-1} in organic electrolyte at an applied current of 0.1 mA cm^2. The cycling performance and coulombic efficiency is also shown in Fig. 13b. The cycle performance was good up to 30 cycles. Beyond 30 cycles, capacity fading was observed (not shown in the figure). Thus, the rate capability in aqueous electrolytes is superior to that in organic electrolytes.

Thermal stability of the electrode material is also a paramount concern for practical application of lithium ion batteries. Figure 14 shows the thermal analysis (thermo-gravimetric analysis—TGA and differential thermal analysis—DTA) of the $LiMnPO_4$ material. In the TGA curve, there is only 1.7% total weight loss when the sample was heated up to 400 °C at a heating rate of 10 °C min^{-1}. There is one broad exothermic peak in the DTA curve which may be attributed to the removal of organic parts of the reactant.

Conclusions

A systematic study of electrochemical behavior of $LiMnPO_4$ cathode material in various aqueous electrolytes has been presented. CV results of $LiMnPO_4$ can be described by reversible reaction system with a resistive behavior. At lower concentrations of lithium ions, $LiMnPO_4$ was found to undergo proton insertion/de-insertion reaction. However, at higher concentrations, lithium insertion becomes the dominating process taking place at the electrode though the interference from proton insertion/de-insertion process cannot be ruled out. Electrochemical lithium ion insertion/de-insertion in $LiMnPO_4$ from aqueous electrolytes has been proved using EIS technique. The cell $LiTi_2(PO_4)_3$/5 M$LiNO_3$/$LiMnPO_4$ delivers a discharge capacity of 84 mAh g^{-1} at $C/5_{rate}$ and the cycling behavior is good over 50 cycles.

Acknowledgements The authors gratefully acknowledge the financial support from the Department of Science and Technology, Government of India. They wish to thank Sri. A. V. S. Murthy, honorary secretary, Rashtreeya Sikshana Samiti Trust, Bangalore, and Dr. P. Yashoda, Principal, S.S.M.R.V. Degree College, Bangalore, for their support and encouragement. They thank the Department of Chemistry, St. Joseph's College, for XRD data.

References

1. Padhi AK, Nanjundaswamy KS, Goodenough JB (1997) J Electrochem Soc 144:1188–1194
2. Manjunatha H, Suresh GS, Venkatesha TV (2011) J Solid State Electrochem 15:431–445
3. Yamada A, Hosoya M, Chung S-C, Hinokuma K, Kudo Y, Liu K-Y (2002) In: Manthiram A, Kumta PN, Sundaram SK, Ceder G (eds) Materials for electrochemical energy conversion and storage. American Ceramic Society, Westerville, pp 189–204
4. Yamada A, Hosoya M, Chung S-C, Hinokuma K, Kudo Y, Liu K-Y (2001) In: Nadri G, Koetz R, Dcrosatti B, Moro PA, Takeuchi ES (eds) Advanced batteries and supercapacitors. The Electrochemical Society, Pennington
5. MacNeil DD, Lu Z, Chen Z, Dahn JR (2002) J Power Sources 108:8–114
6. Yamada A, Chung S-C, Hinokuma K (2001) J Electrochem Soc 148:A224–A229
7. Delacourt C, Poizot P, Morcrette M, Tarascan JM, Masquelier C (2004) Chem Mater 16:93–99
8. Gummov RJ, Thackery MM (1993) J Electrochem Soc 140:3365–3368
9. Guohua L, Ikuta H, Uchida T, Wakihara M (1996) J Electrochem Soc 143:178–182
10. Li G, Azuma H, Tohda M (2002) Electrochem Solid-State Lett 5: A135–A137
11. Yamada A, Chung S-C (2001) J Electrochem Soc 148:A960–A967
12. Bramnik NN, Ehrenberg H (2008) J Alloys Compd 464:259–264
13. Bakenov Z, Taniguchi I (2010) Electrochem Commun 12:75–78
14. Huang H, Yin S-C, Nazar LF (2001) Electrochem Solid-State Lett 4:A170–A172
15. Minakshi M, Singh P, Thurgate S, Prince K (2006) Electrochem Solid-State Lett 9:A471–A474
16. Minakshi M, Pandey A, Blackford M, Ionescu M (2010) Energy Fuel 24:6193–6197
17. Pol VG, Pol SV, Gedanken A, Kessler VG, Seisenbaeva GA, Sung M, Asai S (2005) J Phys Chem B 109:6121–6125
18. Pol SV, Pol VG, Kessler VG, Seisenbaeva GA, Sung M, Asai S, Gedanken A (2004) J Phys Chem B 108:6322–6327
19. Pol SV, Pol VG, Kessler VG, Seisenbaeva GA, Sung M, Asai S, Gedanken A (2004) Chem Mater 16:1793–1798
20. Pol VG, Pol SV, Gedanken A (2008) J Phys Chem C 112:6627–6637
21. Chen G, Richardson TJ (2009) J Electrochem Soc 156:A756–A762
22. Delacourt C, Poizot P, Morcrette M, Tarascon JM, Masquelier C (2004) Chem Mater 16:93–99

23. Yu DYW, Fietzek C, Weydanz W, Donoue K, Inoue T, Kurokawa H, Fujitani S (2007) J Electrochem Soc 154:A253–A257
24. Molenda J, Ojczyk W, Swierczek K, Zajac W, Liu R-S Krok F Dygas J (2006) Solid State Ionics 177:2617–2624
25. Lee J-W, Pyun S-II (2004) Electrochim Acta 49:753–761
26. Manjunatha H, Mahesh KC, Suresh GS, Venkatesha TV (2011) Electrochim Acta 56:1439–1446
27. Shivashankaraiah RB, Manjunatha H, Mahesh KC, Suresh GS, Venkatesha TV (2011) J Solid State. Electrochem. doi:10.1007/s10008-011-1520-7
28. Manjunatha H, Venkatesha TV, Suresh GS (2011) Electrochim Acta 58:247–257
29. Sinha NN, Ragupathy P, Vasan HN, Munichandraiah N (2008) Int J Electrochem Soc 3:691–710
30. Ho C, Raistrick ID, Huggins RA (1980) J Electrochem Soc 127:343–350
31. Wang GJ, Qu QT, Wang B, Shi Y, Tian S, Wu YP, Holze R (2009) J Power Sources 189:503–506
32. Wang GJ, Qu QT, Wang B, Shi Y, Tian S, Wu YP, Holze R (2009) Electrochim Acta 54:1199–1203